A Novel Sliding Mode Control Strategy for Remote Area Power Supply Management

Chafik Ed-dahmani[1,*], Morad Hafiane[1], and Ilham Rais[2]
[1] AEEE Department, National Graduate School of Arts and Crafts, Moulay Ismail University, Meknes, Morocco
[2] Department of Electrical Engineering, Mohamadia School of Engineering, Mohammed V University, Rabat, Morocco
Email: c.eddahmani@umi.ac.ma (C.E.-D.), m.hafiane@ensam.ac.ma (M.H.), ilhamrais@research.emi.ac.ma (I.R.)

***Abstract*—This paper introduces a comprehensive Energy Management Strategy (EMS) control for a Remote Area Power Supply (RAPS) system, that includes a wind generation subsystem, a battery bank, and a variable local load. The primary objectives of the EMS control are to meet the load power demand, adapt to wind fluctuations, and extend the battery bank's lifespan. To achieve these objectives, the EMS controller determines the operation modes of the wind generation and battery bank. The study includes a detailed design of a Sliding Mode Controller (SMC) for the boost converter associated with wind power generation. This study offers valuable insights into controlling standalone wind-dominated systems in remote areas, offering solutions to enhance stability by reducing voltage ripple and improving performance through optimizing settling time. Simulations confirm the effectiveness of the proposed technique in managing load and wind variations, outperforming conventional PI controllers.**

***Index Terms*—remote area power supply, sliding mode control, Maximum Power Point Tracking (MPPT), energy management system, boost converter**

I. Introduction

In recent years, there has been a growing focus on use of renewable energy sources for generating electricity. This is because they bring various benefits to the environment, society, and the economy [1, 2]. Among these sources, wind energy is the fastest-growing one [3]. Additionally, the incorporation of wind energy into the power grid has significantly increased over the past decade [4]. With the existing of various architectures, the wind conversion based on Permanent Magnet Synchronous Generator (PMSG) comes with several advantages compared to other solutions [5]. These benefits include a simple design, high power density, excellent efficiency by eliminating gearbox losses, low maintenance needs, and high reliability [6, 7].

The Wind Energy Conversion Systems (WECS) based on PMSG comes as a solution for local power generators to supply isolated or remote regions where access to the electrical grid is not feasible [8–10]. Moreover, the stability of the stand-alone power supply is significantly impacted by the behaviors of wind speed, which is strongly influenced by atmospheric conditions. Consequently, it becomes crucial to explore the integration of a wind power-based energy system with energy storage, as their profiles are complementary [11, 12]. This integration can be considered for constructing a Remote Area Power Supply (RAPS) [13].

Several studies have focused on investigating the control of the RAPS in order to ensure a stable and cost-effective operation in different scenarios. In [14], a Buck-converter is employed as the battery charger for a standalone power system, with the wind turbine operating in Maximum Power Point Tracking (MPPT) mode. In response to challenges posed by unpredictable weather conditions and load fluctuations, the authors of [15] introduced a novel algorithm aimed to optimize the power extraction by regulating the DC link voltage. In [16, 17], the authors present a control strategy designed to ensure an effective power balance between the battery source and load demand. In [18], the authors make a valuable contribution to the feasibility of a wind energy installation paired with battery bank. To attain an efficient operation of MPPT algorithm and minimize stress on the battery, a power flow management controller is integrated with a two-level MPPT controller to optimize performance in the wind power system. In contrast to the aforementioned studies, Watil *et al*. [5] introduce a multi-mode approach to the operation of the RAPS, based on the accessible wind power, load demands, and State Of Charge (SOC) of the battery. The suggested configuration involves a DC-DC Zeta converter as the only controlled converter to simplify the overall control system.

In the RAPS configuration, the inclusion of a battery, along with its charge controller, is essential for energy storage [19, 20]. Nevertheless, the variation on climatic conditions and load demand can lead to inconsistent power flow from wind turbine to other components, potentially leading to degradation of the battery subsystem or unbalanced load supply. To address these challenges, the implementation of Energy Management Strategy (EMS) is imperative [21–23]. This strategy serves to set and regulate the operating parameters of both the wind power and storage subsystems, ensuring the coordination and monitoring of energy flow to achieve equilibrium in supply and load demand while extending the battery's lifetime [24]. Table I gives a comparison between energy management strategies for several existed configuration of others works.

Manuscript received February 5, 2024; revised March 31, 2024; accepted April 8, 2024.

*Corresponding author

TABLE I: COMPARISON OF RECENT PROPOSED EMS

Ref.	RES	RAPS type	ESS	Objectives	Straights	Limitations
[5]	•WECS based on PMSG	DC	•Li-ion battery	•Instantaneous balance of wind turbine power flow to DC load and battery.	-Different control strategies for charge/discharge of bat-tery SOC can attain 100%.	-Use only the WECS -Limited flexibility of RAPS.
[25]	•WECS based on PMSG •PV array	DC or AC	•Battery bank	•Power balancing during operation. •Improving battery life cycle.	-Multi-modes operation	-Existence of PV only not considered.
[26]	•WECS based on PMSG •PV array	DC	•Battery bank	•Min. cost of operation •Improving the life cycle of battery bank. •Balancing control of power flow.	-Multiple's modes to deal with all scenarios.	-In mode 5, the load current can exceed the max. battery current.
[27]	•PV array	DC	•Battery bank •Superca pa-citors	•Efficient dynamic power sharing. •Ensure operation ESS in safety margins.	-Fast regulation of DC bus -Power sharing via Fuzzy logic approach.	-Use only the PV pow-er supply. -Limited flexibility.

This article introduces a novel strategy for optimizing energy distribution among the system components. Based on the accessible wind power, SOC of the battery bank, and load demand, achieving maximum power from the wind turbine may not always be the desired objective. In this context, wind turbine operation is divided into two distinct modes: Power regulation mode and maximum power (MPPT) mode. To facilitate this, an enhanced design of a Sliding Mode Controller (SMC) based on a hysteresis comparator is implemented. As for the battery subsystem, three different charging modes are adopted: maximum current mode, partial current mode, and constant voltage mode. The proposed EMS algorithm ensures smooth transitions between these various operating modes. It is essential to point out that this article primarily focuses on the power control of the wind turbine under diverse scenarios, while the battery charge control algorithm is not within its scope.

The subsequent sections of the paper are structured as follows. Second section presents the mathematical model of the controlled segment. Section III outlines the procedure for implementing the proposed design of the sliding mode controller based on a hysteresis comparator. Section IV is devoted to the development of the proposed energy management strategy. Section V provides numerical simulation results and a detailed discussion. Finally, in Section VI, the paper concludes with conclusions and future prospects.

II. SYSTEM MODELING

The considered RAPS system is shown in Fig. 1, comprises a wind power system based on PMSG connected to the DC bus through a three-phase rectifier and a Boost converter. On the opposite side of the DC bus, a battery bank linked through a bidirectional converter, and an AC load connected to an inverter.

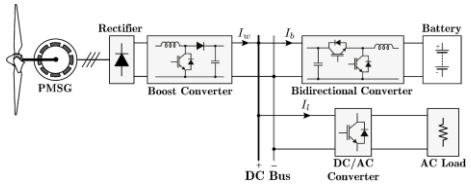

Fig. 1. Structure of RAPS based on wind power-PMSG with energy storage.

A. Wind Power Subsystem

The power extracted by wind turbine P_t can be expressed by the following equation:

$$P_t = \frac{1}{2}\rho A C_p v^3 \tag{1}$$

where ρ is the air density, A is the swept area by the blades of the turbine, R is the blade radius, v is the wind speed, and C_p is the power coefficient. The latter parameter depends mainly on the tip-speed ratio λ and the blade pitch angle β.

For the tip speed ratio is given by

$$\lambda = \frac{R\Omega_m}{v} \tag{2}$$

In optimal conditions, the power extracted by the wind turbine can be maximized for optimal value of the power coefficient $C_{\text{p-max}}$. Therefore, the optimal power of the wind turbine can be given as a nonlinear expression of the mechanical speed Ω_m:

$$P_{t\,\text{opt}} = K_{\text{opt}}\,\Omega_m{}^3 \tag{3}$$

where $K_{\text{opt}} = \frac{1}{2}\rho A C_{p\max}\left(R/\lambda_{\text{opt}}\right)^3$.

The dynamic model of the PMSG is given by the following equations:

$$\begin{cases} \dfrac{di_{\text{sd}}}{dt} = \dfrac{1}{L_s}v_{\text{sd}} - \dfrac{R_s}{L_s}i_{\text{sd}} + w_e\, i_{\text{sq}} \\ \dfrac{di_{\text{sq}}}{dt} = \dfrac{1}{L_s}v_{\text{sq}} - \dfrac{R_s}{L_s}i_{\text{sq}} - w_e\, i_{\text{sd}} - \dfrac{w_e}{L_s}\varphi_{\text{pm}} \\ \dfrac{d\Omega_m}{dt} = \dfrac{1}{J}\left(T_m - T_e\right) - \dfrac{f}{J}\Omega_m \end{cases} \tag{4}$$

where v_{sdq} and i_{sdq} are the dq components of stator voltage and current, respectively. R_s and L_s denote the stator resistance and inductance, respectively, and φ_{pm} is the permanent magnet flux. w_e refers the angular frequency, which is linked to the mechanical speed through the number of pole pairs n_p by the following expression:

$$w_e = n_p\,\Omega_m \tag{5}$$

where T_m is the mechanical torque provided by the WT, while J and f denote the inertia and viscous damping of the rotating components, respectively. The electromagnetic torque, T_e, generated by the PMSG can be given as follows [28]:

$$T_e = \frac{3}{2}\frac{n_p \varphi_{\text{pm}} V_s}{w_e L_s}\sqrt{1-\left(\frac{V_s}{w_e \varphi_{\text{pm}}}\right)^2} \tag{6}$$

From Eq. (6), it can be deduced that there is a minimum mechanical speed, $\Omega_{\text{cut-in}}$, at which the PMSG is unable to produce energy. This holds true for any given value of the stator voltage, V_s. Consequently, $\Omega_{\text{cut-in}}$ can be determined from Eq. (5) and Eq. (6) as follows:

$$\Omega_{\text{cut-in}} = \frac{V_s}{n_p \varphi_{\text{pm}}} \tag{7}$$

B. DC Boost Converter Model

The state model of DC-boost converter can be obtained from the instantaneous values by [29]:

$$\begin{cases} \dfrac{dV_{\text{bus}}}{dt} = \dfrac{1}{C_b}(1-u)I_{\text{in}} - \dfrac{1}{C_b}I_w \\ \dfrac{dI_{\text{in}}}{dt} = \dfrac{1}{L}V_{\text{in}} - \dfrac{1}{L}(1-u)V_{\text{bus}} \\ i_{\text{Cin}} = I_{\text{in}} - i_L = C_{\text{in}}\dfrac{dV_{\text{in}}}{dt} \end{cases} \tag{8}$$

where V_{in} and V_{bus} represent the terminal voltage of the rectifier and the DC bus voltage, respectively. I_w and I_{in} denote the current provided by WT subsystem to the DC bus and the input current Boost converter. The command signal of the DC converter is represented by u={0,1}. Additionally, L and C_b are the inductance and output capacitor of the converter. For i_{Cin} and i_L are the current components through the input capacitor (C_{in}) and inductance, respectively.

The average values of input and output voltages for DC boost converter related by: $V_{\text{bus}} = V_{\text{in}}/(1-D)$, where D is the duty cycle. The output power of the PMSG (V_s, i_{sdq}) can be related to the injected power on the DC bus (V_{bus}, I_w) by the following equations:

$$\begin{cases} V_s = \dfrac{\pi}{3\sqrt{3}}(1-D)V_{\text{bus}} \\ I_w = \dfrac{\pi}{2\sqrt{3}}(1-D)\sqrt{i_{\text{sd}}^2 + i_{\text{sq}}^2} \end{cases} \tag{9}$$

From Eq. (9), the injected current indirectly depends on the duty cycle D.

III. Control Algorithms and Energy Management Strategy

A. Overview of EMS and Policy

Essentially, the operational modes are selected in accordance with the energy equilibrium established between the WT and the total energy demand, which includes both the load demand and the requisite power for recharging the battery [30].

In the design of the EMS control unit, the battery is in a charging mode by default. This decision stems from the battery's sizing, allowing it to sustain autonomy for multiple days, depending on wind conditions and load power demand. Importantly. This design choice does not limit the proposed control framework. If necessary, the outcomes detailed below can be easily expanded by incorporating a solar power subsystem as an additional and complementary energy source.

The control objectives are dynamically adjusted at the base of the maximum available wind power, SOC of the battery, and load power demand (P_{load}). Based on the values of the parameters mentioned previously, three principal control objectives are highlighted:

- Promoting the supply of load demand with power generated by a wind turbine.
- Ensuring system stability through DC bus voltage regulation.
- Enhancing the performance and extending the lifespan of the battery. The total power demand by the load and the battery can be defined by the following equation:

$$P_{\text{total demand}} = V_{\text{bus}}\left(i_{b\,\text{ref}} + i_{\text{load}}\right) \tag{10}$$

where i_{bref} the battery reference current describes its charge state. To ensure one of the control objectives, the SOC is kept within specific limits $\text{SOC}_{\text{min}} \leq \text{SOC} \leq \text{SOC}_{\text{max}}$ [31]. Therefore, a management strategy is essential to address various scenarios that may arise due to fluctuations in wind speed, load demand, or changes in SOC of the battery.

The optimal power is calculated by

$$P_{\text{opt}} = P_{\text{MPP}} - P_{\text{losses}} \tag{11}$$

P_{losses} is the losses through the PMSG, it is expressed by the following equation:

$$P_{\text{losses}} = \frac{3}{2}R_s\left(i_{\text{sd}}^2 + i_{\text{sq}}^2\right) \tag{12}$$

To attain the specified control objectives, an Energy Management System (EMS) is formulated, relying on four distinct modes of operation. The flow chart illustrating the adopted EMS is presented in Fig. 2.

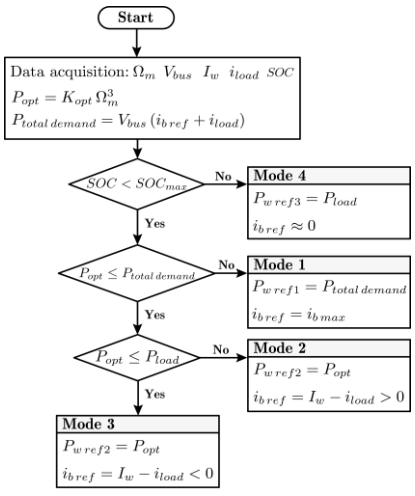

Fig. 2. Flowchart of the proposed EMS.

The defined operation modes are elucidated as follows:

Mode 1: The Wind Turbine (WT) operates in power regulation mode; the operating point is different from the Maximum Power Point (MPP). The power generated is regulated to a reference value defined by $P_{w\,\mathrm{ref}}$.

Meanwhile, the battery operates in charging mode, specifically in constant current control mode. To prevent potential damage, the charging current must follow a constant reference corresponding to the maximum battery current.

$$i_{b\,\mathrm{ref}} = i_{b\,\max} > 0 \tag{13}$$

$$P_{w\,\mathrm{ref}} = P_{\mathrm{total\,demand}} = V_{\mathrm{bus}}\left(i_{b\,\mathrm{ref}} + i_{\mathrm{load}}\right) \tag{14}$$

Mode 2: WT is unable to supply the load demand and charge the battery with is maximum admissible current. Then, WT extracts the maximum available power from wind (MPPT mode); Battery is in partial charging mode (constant current regulation).

$$P_{\mathrm{opt}} \geq P_{\mathrm{load}} \tag{15}$$

$$i_{b\,\mathrm{ref}} = I_w - i_{\mathrm{load}} < i_{b\,\max} \tag{16}$$

Mode 3: The load demand exceeds the maximum available power from the wind. Consequently, WT operates in Maximum Power Point Tracking (MPPT) mode, while the Battery is in partial discharging mode. The residual power, the difference between the power extracted by the wind power subsystem and the load power (P_{opt}–P_{load}), is provided by the battery without excessive discharge. In this scenario, the DC bus voltage is regulated to stabilize the power flow.

$$P_{\mathrm{opt}} < P_{\mathrm{load}} \tag{17}$$

Mode 4: WT is in power regulation mode; it supplies the load power; Battery is considered in full charge (SOC=$\mathrm{SOC}_{\max}$), (battery voltage regulation), the battery charging current is neglected.

B. Boost Controller Design

Various control strategies are employed to regulate the boost voltage, aligning it with the reference from the MPPT algorithm [32]. These strategies try to mitigate disturbances from both the load and changes in wind speed. The Proportional-Integral (PI) controller is formulated using a linear model of the WT subsystem, typically centered around a specific operating point such as the Maximum Power Point (MPP) [33]. To maintain consistent performance across the entire operational range, it is essential to design controllers that are robust and not exclusively reliant on linearized models.

This paper presents an approach based on the methodology discussed in [34], which employs sliding-mode techniques to control the PV voltage and reject disturbances caused by the load imbalance and fluctuations in solar irradiance. Expanding on the referenced work, the formulation of a control law is undertaken to ensure system stability, achieve the desired settling time, and eliminate overshoot should integrate the boost voltage error (V_{in}–V_{in}^{*}) and the voltage derivative into the sliding surface *z*, as expressed in Eq. (18).

$$z = K_1\left(V_{\mathrm{in}} - V_{\mathrm{in}}^{*}\right) + K_2\frac{dV_{\mathrm{in}}}{dt} \tag{18}$$

The primary advantage of employing such a sliding surface is in the regulating the boost voltage without the need for supplementary controllers relying on linearized models. This paper provides a novel analysis and design approach for the control system, ensuring the stability and precision during in tracking the reference voltage.

The controller structure is illustrated in Fig. 3. The voltage reference V_{in}^{*} is supplied by a power controller, with the power reference selected by the EMS based on the operation mode. The dynamic model of the boost converter is expressed by Eq. (8).

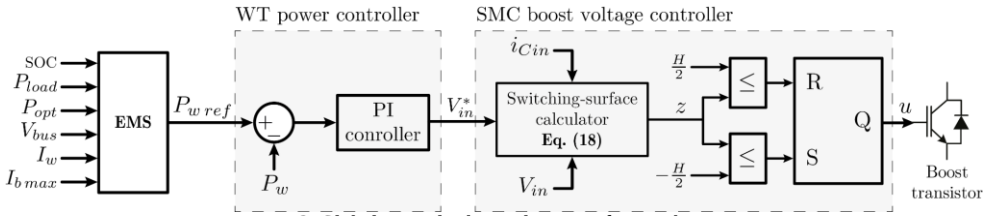

Fig. 3. Global control scheme diagram of WT subsystem.

The building of a stable sliding mode controller necessitates three conditions: transversality, equivalent control, and convergence [35]. By applying the previous mentioned conditions, an approach is developed to design a control structure for the Boost converter with respect to the desired performance.

These conditions are employed to formulate a design approach for the control system, ensuring the desired performance criteria for the WT-boost voltage.

C. Transversality Condition

This condition aims to rely the dynamic evolution of sliding surface z to the control signal command u of the Boost converter [36], the established relation can be expressed as:

$$\frac{d\left(dz/dt\right)}{du} \neq 0 \tag{19}$$

To validate the condition stated in Eq. (19), the derivative

with respect to time of the sliding surface is expressed as:

$$\frac{dz}{dt} = K_1\left(\frac{dV_{\text{in}}}{dt} - \frac{dV_{\text{in}}^*}{dt}\right) + K_2\left(\frac{dI_{\text{in}}}{dt} - \frac{di_L}{dt}\right) \quad (20)$$

By replacing Eq. (8) in Eq. (20), the initial condition becomes:

$$\frac{dz}{dt} = K_1\left(\frac{dV_{\text{in}}}{dt} - \frac{dV_{\text{in}}^*}{dt}\right) + K_2\frac{dI_{\text{in}}}{dt} - \frac{K_2}{L}\left(V_{\text{in}} - V_{\text{bus}}(1-u)\right) \quad (21)$$

The analysis of the transversality condition involves taking the derivative of Eq. (21) with respect to u, resulting in Eq. (22). Since L and V_{bus} are strictly positive, the condition of transversality is satisfied when $K_2 \neq 0$.

$$\frac{d\left(dz/dt\right)}{du} = -\frac{K_2}{L} \neq 0 \quad (22)$$

D. Convergence Condition

In this scenario, the system's capability to achieve the desired state (z=0) is assessed. A hysteresis comparator is employed to generate the control command u for the DC boost converter. In this application, the sliding surface z is bounded within the limits of $-H/2$ and $H/2$, where H is the hysteresis bound. In this case, the control command u is generated based on the following conditions.

$$\begin{cases} z \leq -H/2 \rightarrow u = 1 \\ z \geq H/2 \rightarrow u = 0 \end{cases} \quad (23)$$

In this investigation, the limitations on u outlined in Eq. (23) are dictated by the positive fulfillment of the initial condition presented in Eq. (19). This is established for a negative value of K_2.

E. Equivalent Control Condition

The equivalent control condition is validated when z=0, and this condition is achieved for an equivalent value of the control command u_{eq}. In a DC converter, the average value of the control signal is the duty cycle. Applying this condition leads to Eq. (24):

$$z = 0 \rightarrow i_{\text{Cin}} = C_{\text{in}}\frac{dV_{\text{in}}}{dt} = -\frac{K_1}{K_2}\left(V_{\text{in}} - V_{\text{in}}^*\right) \quad (24)$$

By applying the Laplace transform for the previous equation, it leads to:

$$\frac{V_{\text{in}}(s)}{V_{\text{in}}^*(s)} = \frac{1}{C_{\text{in}}\left(K_2/K_1\right)s + 1} \quad (25)$$

Eq. (25) illustrates the equivalent transfer condition between the boost terminal voltage and its reference. By selecting the equivalent pole, the stability condition conduct to $K_2/K_1>0$. Consequently, K_1 shares the same sign as K_2, which is negative as deduced in the convergence condition.

Determination of K_2: In steady state, the SMC ensures that V_{in} equals V_{in}^*. According to Eq. (18) and Eq. (23), the hysteresis band of the sliding surface transforms into $-H/2 \leq K_2 i_{\text{Cin}} \leq H/2$ [34]. During operation, the input capacitor current i_{Cin} oscillates between the lower and upper boundaries of the steady-state current, representing the current ripple Δi_{Cin}. Consequently, the magnitude of K_2 can be determined by the following expression:

$$\left|K_2\right| = \frac{H}{\Delta i_{\text{Cin}}} \quad (26)$$

In practical constraints, Δi_{Cin} is selected to guarantee Continuous Conduction Mode (CCM), thereby avoiding a significant ripple in V_{in}.

Determination of K_1: With K_2 determined, K_1 is established by employing the Metaheuristic Particle Swarm Optimization Algorithm (MPSOA), while considering the constraints outlined in the previous conditions.

The MPSOA is commonly employed for optimization problems across diverse engineering domains, recognized for its efficiency and computational speed in exploring global optimal solutions. This algorithm is formulated based on the collective behavior observed in a swarm of N_p particles, each representing a candidate solution [37].

The MPSOA holds a notable advantage as it can be employed for nonlinear, non-differentiable problems. In a nonlinear and uncertain context, the goal of this study is to determine the optimal value of K_1 to achieve optimal reference tracking.

The fitness function chosen in this context is the integral absolute value of the error (IAE) of the input Boost converter voltage. The fitness function is expressed in the following equation:

$$\text{IAE} = \int |V_{\text{in}}^* - V_{\text{in}}|\, dt \quad (27)$$

The various steps employed in the MPSOA-based tuning of the proposed SMC are depicted in Fig. 4.

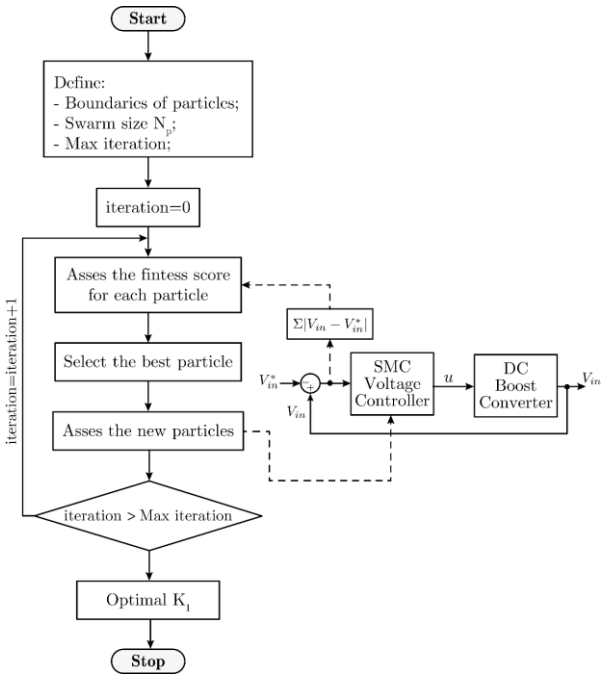

Fig. 4: Flow chart of K_1 determination based on MPSOA.

Design methodology: The voltage controller design relies on specifying the inductor current ripples Δi_L. Given that the inductor L and the input capacitor C_{in} constitute a second-order LC filter [38], with taking into account the small-ripple of the input voltage, the magnitudes of the current ripples are identical for both the inductor (Δi_L) and the capacitor (Δi_{Cin}), i.e. $\Delta i_{Cin}=\Delta i_L$. Therefore, K_2 is determined from (26) according to the specified hysteresis band (H) and Δi_{Cin} value. Meanwhile, K_1 is determined directly through MPSOA.

IV. Simulation Results and Discussion

The discussed control structure associated to the EMS for the considered RAPS system have been tested through detailed modeling in the MATLAB/Simulink platform. These simulations use a high-precision model that incorporates the entire system dynamics, which increases their consistency with real-world scenarios. To closely replicate the actual system, a small sample time ($Ts=10\,\mu s$) is adopted in the simulations, enabling the capture of real-time behavior in the components. The system under consideration is configured using the numerical parameter values specified in Table 22 and Table 33.

Table II: RAPS Based on WT Subsystem Characteristics

	Parameter	Value
Turbine	Nominal power	3.3 kW
	Blade Radius	1.43 m
	Nominal wind speed	12 m/s
PMSG	Stator resistance	0.24 Ω
	Stator inductance	0.395 mH
	Number of pole pairs	4
	Nominal speed	314 rad/s
	PM Rotor flux	0.1194
	Total inertia	0.0027 kg.m ²
	Total viscous damping	0.00049 N.m.s
Boost converter	Inductor	2.7 mH
	Input capacitor	150 µF
	Output capacitor	660 µF
Battery	Nominal capacity	100 Ah
	Boundaries of SOC	20% and 80%
	Internal resistance	0.0048 Ω
	Max. discharge current	20 A

Table III: The Parameters of Controllers.

Controller parameter		Value
Tuned PI controller		k_p=0.4; k_i=35
SMC controller	Gains	K_1=5.709; K_2=2.3
	Hysteresis bounda	H=1.667
MPSOA	Swarm size	30
	Max. Iteration	5

To highlight the performance of the suggested control strategies, two scenarios involving variations in wind speed and the operation mode of the WT subsystem were simulated.

In the initial simulation scenario, the wind speed is set at 12 m/s, and the WT operates at the Maximum Power Point (MPP). The responses of the input voltage of the boost converter, controlled by both the PI (with the gains K_p and K_i are defined in Table II) controller and proposed SMC, are depicted in Fig. 5.

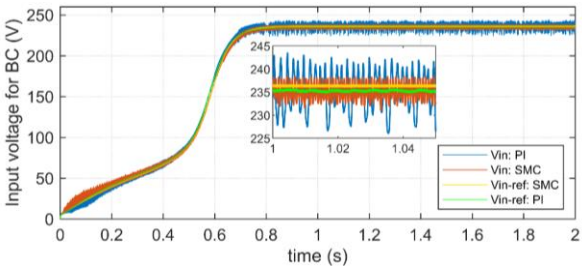

Fig. 5. Input voltage of Boost converter responses.

It can be seen that all controllers successfully track their reference power with the same settling time (t = 0.75s) and a steady-state voltage of 236.4 V. This voltage is generated by the Perturb and Observe (PO) algorithm (depicted in the green signal) for the PI voltage controller, and by a tuned PI controller (shown in the yellow signal) for the proposed control structure. For the voltage ripples, the real response reveals that the proposed Sliding Mode Controller (SMC) (indicated by the brown signal) surpasses the PI controller (represented by the blue signal), presenting ΔV_{in} = 5.8V compared to ΔV_{in} = 14.6V. It is important to note that the relatively high settling time is attributed to the input capacitor C_{in} of the boost converter.

In the second scenario, the characteristics of the proposed control structure and Energy Management Strategy (EMS) are evaluated based on the actual behaviors of wind speed and load power demand, incorporating time-intervals of both sufficient and insufficient power generation. Fig. 6 illustrates the wind speed (v[m/s]) fluctuating between 5.84–12 m/s, with a mean of 9.1 m/s. In Fig. 7, the AC load power demand connected to the DC bus through inverter is depicted. The changes in its value denote load connections or disconnections.

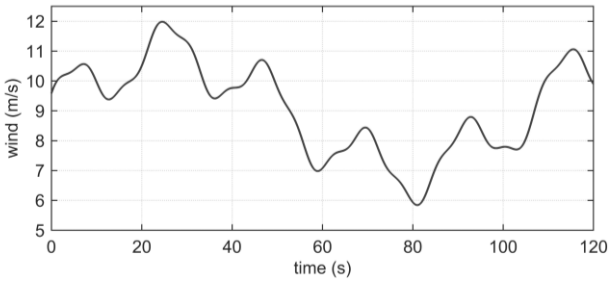

Fig. 6. Wind speed signal v[m/s].

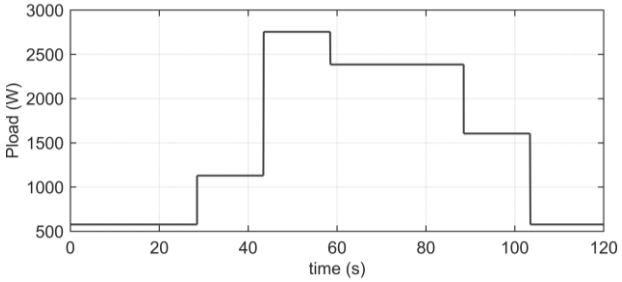

Fig. 7. Load power demand P_{load} [W].

In Fig. 8, the temporal dynamics of powers for various components of the examined RAPS are illustrated. This

includes the power generation of WT, the power demand, and the supplied power to the load from the battery. The figure demonstrates that the generated power precisely matches the total power demand, with the exception of periods of insufficient generation (P_w<P_{load}). Within these intervals, the battery defers its recharging cycle and supplements power generation by giving its stored energy. By analyzing the real-time values of P_w, P_{load}, and SOC, the Energy Management System identifies the operational mode of the RAPS, as depicted in Fig. 9. Mode 4 is not included, since it requires SOC=SOC_{max}, which implies a long time period to reach this state for the battery during simulation phase.

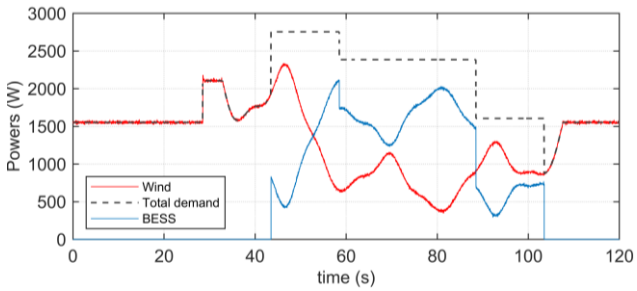

Fig. 8. Power curves, wind generation (red), total demand (dashed), and battery (blue).

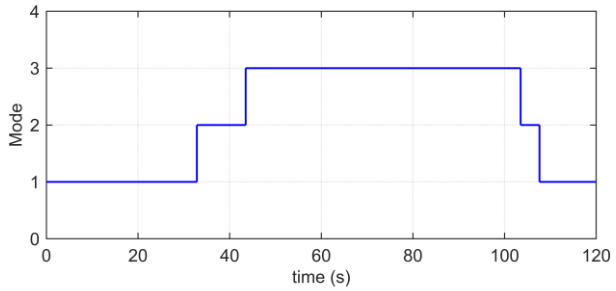

Fig. 9. Mode of operation of RAPS.

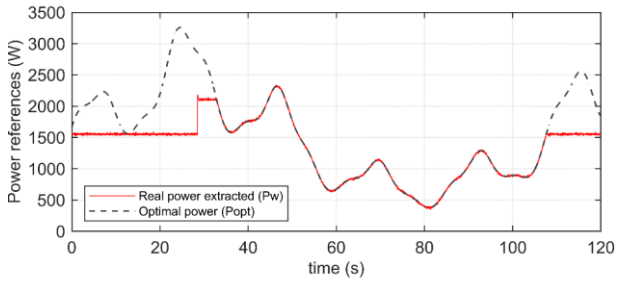

Fig. 10. Actual WT generation power versus its optimal curve.

Finally, the maximum and the real wind power are shown in Fig. 10. The wind turbine subsystem in modes 2 and 3 tracks the optimal generation reference, as described in the flow chart of the EMS in Fig. 2. It is important to mention that at $t \cong 34.28$ s , the WT subsystem tracks the optimal power P_{opt}, and the battery is charged using partial current (constant current mode). From $t \cong 45$ s to $t \cong 105$ s , the WT remains in MPPT mode control, while the battery supplies the complementary power to satisfy the load demand. Between $t \cong 105s$ and $t \cong 109.4s$, the load demand is decreased, leading the battery to switch from discharging to partial charging mode. Subsequently, as the wind speed increases, the WT's generation power becomes sufficient to supply the load demand and charge the battery with the maximum admissible current.

V. Conclusion

The effectiveness of an electric generation system significantly depends on the presence of a customized EMS control capable of governing the various subsystems involved. The proposed EMS has proven high competence in managing and coordinating the operation of the components constituting the considered RAPS. It offers a flexible decision-making framework for determining the operational mode of each electrical subsystem. A salient feature of this system is the proposal of reliable and clear criteria based on measurable system variables (specifically, SOC, rotational speed, wind and load demand powers) for the EMS decision algorithms.

An enhanced method for the design of input voltage controller of the Boost converter based on the sliding mode controller in a RAPS system based on PMSG has been introduced. The input voltage of the boost converter effectively tracks the reference set by the power controller, demonstrating a predetermined settling time and absence of overshoot, also, it exhibits a robustness against wind variations and load balance. The proposed controller with the selected sliding surface reduces the complexity comparing to other similar solutions that uses a cascaded loop. The exclusion of linearization process is a crucial aspect of the enhanced method, ensuring the use of the analytical expressions across the entire operational range, as long as the sliding regime is sustained.

Finally, to expand on the work discussed in this paper, additional tasks can be explored, including: adding a PV subsystem, comparing the achieved results with other advanced control techniques such as integral-SMC, model predictive control, etc., and investigating the system stability in the presence of faults in its various components. An experimental validation of the presented findings will also be a focus of our future investigation.

Conflict of Interest

The authors declare no conflict of interest.

Author Contributions

Chafik Ed-dahmani conceptualized, developed, implemented, and wrote the initial draft of the article. Morad Hafiane and Ilham Rais, reviewed, validated, edited, and finalized the work. All authors have approved the final version.

Acknowledgement

The Authors wish to thank the University of Moulay Ismail, and Mohamed 5 University for their support.

References

[1] A. Pfeifer, G. Krajačić, D. Ljubas, and N. Duić, "Increasing the integration of solar photovoltaics in energy mix on the road to low emissions energy system—Economic and environmental implications," *Renewable Energy*, vol. 143, pp. 1310–1317, Dec. 2019. doi: 10.1016/j.renene.2019.05.080

[2] M. S. Javed, T. Ma, J. Jurasz, F. A. Canales, S. Ahmed, and Y. Zhang, "Economic analysis and optimization of a renewable energy-based power supply system with different energy storages for a remote island," *Renewable Energy*, vol. 164, pp. 1376–1394, Feb. 2021. doi: 10.1016/j.renene.2020.10.063

[3] L. Xiong, P. Li, F. Wu, M. Ma, M. W. Khan, and J. Wang, "A coordinated high-order sliding mode control of DFIG wind turbine for power optimization and grid synchronization," *International Journal of Electrical Power & Energy Systems*, vol. 105, pp. 679–689, Feb. 2019. doi: 10.1016/j.ijepes.2018.09.008

[4] A. Dida, F. Merahi, and S. Mekhilef, "New grid synchronization and power control scheme of doubly-fed induction generator-based wind turbine system using fuzzy logic control.," *Computers & Electrical Engineering*, vol. 84, 106647, Jun. 2020. doi: 10.1016/j.compeleceng.2020.106647

[5] A. Watil, A. El Magri, R. Lajouad, A. Raihani, and F. Giri, "Multi-mode control strategy for a stand-alone wind energy conversion system with battery energy storage," *Journal of Energy Storage*, vol. 51, 104481, Jul. 2022. doi: 10.1016/j.est.2022.104481

[6] C. Eddahmani, "A Comparative Study of Fuzzy Logic Controllers for Wind Turbine Based on PMSG," *International Journal of Renewable Energy Research (IJRER)*, vol. 8, no. 3, pp. 1386–1392, Sep. 2018.

[7] C. Ed-dahmani, H. Mahmoudi, and M. Elazzaoui, "Direct torque control of permanent magnet synchronous motors in MATLAB/SIMULINK," in *2016 International Conference on Electrical and Information Technologies (ICEIT)*, May 2016, pp. 452–457. doi: 10.1109/EITech.2016.7519641

[8] X.-M. Lin, N. Kireeva, A. V. Timoshin, A. Naderipour, Z. Abdul-Malek, and H. Kamyab, "A multi-criteria framework for designing of stand-alone and grid-connected photovoltaic, wind, battery clean energy system considering reliability and economic assessment," *Energy*, vol. 224, 120154, Jun. 2021. doi: 10.1016/j.energy.2021.120154

[9] D.-A. Ciupageanu, L. Barelli, A. Ottaviano, D. Pelosi, and G. Lazaroiu, "Innovative power management of hybrid energy storage systems coupled to RES plants: The simultaneous perturbation stochastic approximation approach," Nov. 17, 2023.

[10] D.-A. Ciupageanu, L. Barelli, and G. Lazaroiu, "Design of a Fuzzy Logic Controller for a Remote Power Application," in *2019 IEEE PES Innovative Smart Grid Technologies Europe (ISGT-Europe)*, Sep. 2019, pp. 1–5. doi: 10.1109/ISGTEurope.2019.8905519

[11] X. Xu, W. Hu, D. Cao, Q. Huang, and Z. Liu, "Scheduling of wind-battery hybrid system in the electricity market using distributionally robust optimization," *Renewable Energy*, vol. 156, pp. 47–56, Aug. 2020. doi: 10.1016/j.renene.2020.04.057

[12] A. A. A. Alahmadi, Y. Belkhier, N. Ullah, H. Abeida, M. S. Soliman, Y. S. Khraisat, and Y. M. Alharbi, "Hybrid Wind/PV/Battery Energy Management-Based Intelligent Non-Integer Control for Smart DC-Microgrid of Smart University," *IEEE Access*, vol. 9, pp. 98948–98961, 2021. doi: 10.1109/ACCESS.2021.3095973

[13] H. Kord and S. M. Barakati, "Design an adaptive sliding mode controller for an advanced hybrid energy storage system in a wind dominated RAPS system based on PMSG," *Sustainable Energy, Grids and Networks*, vol. 21, p. 100310, Mar. 2020. doi: 10.1016/j.segan.2020.100310

[14] K.-Y. Lo, Y.-M. Chen, and Y.-R. Chang, "MPPT battery charger for stand-alone wind power system," *IEEE Transactions on Power Electronics*, vol. 26, no. 6, pp. 1631–1638, Jun. 2011. doi: 10.1109/TPEL.2010.2088405

[15] C. N. Bhende, S. Mishra, and S. G. Malla, "Permanent magnet synchronous generator-based standalone wind energy supply system," *IEEE Transactions on Sustainable Energy*, vol. 2, no. 4, pp. 361–373, Oct. 2011. doi: 10.1109/TSTE.2011.2159253

[16] D. K. V. Sagiraju, Y. P. Obulesu, and S. B. Choppavarapu, "Dynamic performance improvement of standalone battery integrated PMSG wind energy system using proportional resonant controller," *Engineering Science and Technology, an International Journal*, vol. 20, no. 4, pp. 1353–1365, Aug. 2017. doi: 10.1016/j.jestch.2017.03.010

[17] C. Wang, Z. Zhang, O. Abedinia, and S. G. Farkoush, "Modeling and analysis of a microgrid considering the uncertainty in renewable energy resources, energy storage systems and demand management in electrical retail market," *Journal of Energy Storage*, vol. 33, 102111, Jan. 2021. doi: 10.1016/j.est.2020.102111

[18] S. Belaid, D. Rekioua, A. Oubelaid, D. Ziane, and T. Rekioua, "A power management control and optimization of a wind turbine with battery storage system," *Journal of Energy Storage*, vol. 45, 103613, Jan. 2022. doi: 10.1016/j.est.2021.103613

[19] D. Groppi, A. Pfeifer, D. A. Garcia, G. Krajačić, and N. Duić, "A review on energy storage and demand side management solutions in smart energy islands," *Renewable and Sustainable Energy Reviews*, vol. 135, 110183, Jan. 2021. doi: 10.1016/j.rser.2020.110183

[20] R. Gugulothu, B. Nagu, and D. Pullaguram, "Energy management strategy for standalone DC microgrid system with photovoltaic/fuel cell/battery storage," *Journal of Energy Storage*, vol. 57, 106274, Jan. 2023. doi: 10.1016/j.est.2022.106274

[21] F. Valenciaga, P. F. Puleston, and P. E. Battaiotto, "Variable structure system control design method based on a differential geometric approach: application to a wind energy conversion subsystem," *IEE Proceedings - Control Theory and Applications*, vol. 151, no. 1, pp. 6–12, Jan. 2004. doi: 10.1049/ip-cta:20030976

[22] M. H. Nazari, M. Bagheri-Sanjareh, and S. H. Hosseinian, "A new method for energy management of residential microgrid for sizing electrical and thermal storage systems," *Sustainable Cities and Society*, vol. 76, 103482, Jan. 2022. doi: 10.1016/j.scs.2021.103482

[23] G. Chaudhary, J. J. Lamb, O. S. Burheim, and B. Austbø, "Review of energy storage and energy management system control strategies in microgrids," *Energies*, vol. 14, no. 16, Art. no. 16, Jan. 2021. doi: 10.3390/en14164929

[24] R. G. Allwyn, A. Al-Hinai, and V. Margaret, "A comprehensive review on energy management strategy of microgrids," *Energy Reports*, vol. 9, pp. 5565–5591, Dec. 2023. doi: 10.1016/j.egyr.2023.04.360

[25] A. Watil, A. El Magri, R. Lajouad, A. Raihani, and F. Giri, "Multi-mode control strategy for a stand-alone wind energy conversion system with battery energy storage," *Journal of Energy Storage*, vol. 51, 104481, 2022. doi: 10.1016/j.est.2022.104481

[26] F. Ez-zahra Lamzouri, E.-M. Boufounas, and A. E. Amrani, "Efficient energy management and robust power control of a stand-alone wind-photovoltaic hybrid system with battery storage," *Journal of Energy Storage*, vol. 42, 103044, 2021. doi: 10.1016/j.est.2021.103044

[27] M. Benzaouia, B. Hajji, A. Rabhi, S. Benzaouia, and A. Mellit, "Real-time Super Twisting Algorithm based fuzzy logic dynamic power management strategy for Hybrid Power Generation System," *Journal of Energy Storage*, vol. 65, 107316, 2023. doi: 10.1016/j.est.2023.107316

[28] F. Ez-zahra Lamzouri, E.-M. Boufounas, and A. E. Amrani, "Efficient energy management and robust power control of a stand-alone wind-photovoltaic hybrid system with battery storage," *Journal of Energy Storage*, vol. 42, 103044, Oct. 2021. doi: 10.1016/j.est.2021.103044

[29] M. Benzaouia, B. Hajji, A. Rabhi, S. Benzaouia, and A. Mellit, "Real-time Super Twisting Algorithm based fuzzy logic dynamic power management strategy for Hybrid Power Generation System," *Journal of Energy Storage*, vol. 65, 107316, Aug. 2023. doi: 10.1016/j.est.2023.107316

[30] M. F. Roslan, M. A. Hannan, P. Jern Ker, R. A. Begum, T. Indra Mahlia, and Z. Y. Dong, "Scheduling controller for microgrids energy management system using optimization algorithm in achieving cost saving and emission reduction," *Applied Energy*, vol. 292, 116883, Jun. 2021. doi: 10.1016/j.apenergy.2021.116883

[31] "IEEE Guide for Optimizing the Performance and Life of Lead-Acid Batteries in Remote Hybrid Power Systems," *IEEE Std 1561-2019 (Revision of IEEE Std 1561-2007)*, pp. 1–34, Jun. 2019. doi: 10.1109/IEEESTD.2019.8736085

[32] S. Belhimer, M. Haddadi, and A. Mellit, "A novel hybrid boost converter with extended duty cycles range for tracking the maximum power point in photovoltaic system applications," *International Journal of Hydrogen Energy*, vol. 43, no. 14, pp. 6887–6898, Apr. 2018. doi: 10.1016/j.ijhydene.2018.02.136

[33] N. Femia, G. Petrone, G. Spagnuolo, and M. Vitelli, "Optimization of perturb and observe maximum power point tracking method," *IEEE Transactions on Power Electronics*, vol. 20, no. 4, pp. 963–973, Jul. 2005. doi: 10.1109/TPEL.2005.850975

[34] D. G. Montoya, C. A. Ramos-Paja, and R. Giral, "Improved Design of Sliding-Mode Controllers Based on the Requirements of MPPT Techniques," *IEEE Transactions on Power Electronics*, vol. 31, no. 1, pp. 235–247, Jan. 2016. doi: 10.1109/TPEL.2015.2397831

[35] H. Sira-Ramirez, "Sliding motions in bilinear switched networks," *IEEE Transactions on Circuits and Systems*, vol. 34, no. 8, pp. 919–933, 1987. doi: 10.1109/TCS.1987.1086242

[36] S.-C. Tan, Y. M. Lai, and C. K. Tse, "General Design Issues of Sliding-Mode Controllers in DC–DC Converters," *IEEE Transactions on Industrial Electronics*, vol. 55, no. 3, pp. 1160–1174, 2008. doi: 10.1109/TIE.2007.909058

[37] A. Dali, S. Abdelmalek, A. Bakdi, and M. Bettayeb, "A novel effective nonlinear state observer based robust nonlinear sliding mode controller for a 6 kW Proton Exchange Membrane Fuel Cell voltage regulation," *Sustainable Energy Technologies and Assessments*, vol. 44, p. 100996, 2021. doi: 10.1016/j.seta.2021.100996

[38] R. W. Erickson and D. Maksimovic, *Fundamentals of Power Electronics*. Springer Science & Business Media, 2007.

Chafik Ed-dahmani received his engineering degree in mechatronics from University of Abdelmalek Essaadi in 2014, and Ph.D. degree from the University of Mohamed 5-Rabat, Morocco. Currently he is an assistant professor in National Graduate School of Arts and Crafts-Meknès, Morocco. His research interests in renewable energy system conversion, Controlling power converters, and microgrids.

Morad Hafiane received his engineering degree in electromechanical in 2011, and Ph.D. degree in 2018 from University of Moulay Ismail Meknes, Morocco. Currently he is an assistant professor in National Graduate School of Arts and Crafts-Meknès, Morocco. His research interests in renewable energy, Internet of Things (IoT) digital solutions.

Ilham Rais received his engineering degree in Electrical from University of Sultan Moulay Slimane in 2014, and Ph.D. degree in 2020 from University of Mohamed 5-Rabat, Morocco. Currently she is a Professional Trainer at the industrial specialized institute-Marrakech, Morocco. Her research interests in renewable energy conversion systems, electrical energy storage systems, power electronics.